**Proceedings of ASME 2014 Dynamic Systems and Control Conference**
**DSCC 2014**
**October 22-24, 2014, San Antonio, Texas, USA**

**DSCC2014-6362**

# FUEL CONSUMPTION OPTIMIZATION OF HEAVY-DUTY VEHICLES: AN ANALYTICAL APPROACH

**Chaozhe R. He***
Department of Mechanical Engineering
University of Michigan
Ann Arbor, Michigan 48109
Email: hchaozhe@umich.edu

**Gábor Orosz**
Department of Mechanical Engineering
University of Michigan
Ann Arbor, Michigan 48109
Email: orosz@umich.edu

## ABSTRACT

*In this paper, we establish a mathematical framework that allows us to optimize the speed profile and select the optimal gears for heavy-duty vehicles. The key idea is to solve the analogous boundary value problem analytically for a simple scenario (linear damped system with quadratic elevation profile) and use this result to initialize a numerical continuation algorithm. Then the numerical algorithm can be used to gradually introduce nonlinearities (air resistance, engine saturation), implement data-based elevation profiles, and incorporate external perturbations (wind, traffic). This approach enables real-time optimization in dynamic traffic conditions, therefore may be implemented on board.*

## 1 INTRODUCTION

A large percentage of freight transport nowadays is carried out by heavy-duty vehicles (HDVs). According to U.S. Department of Energy [1], more than 10 million registered HDVs deliver 70% of the domestic freight transport counted in value and they are responsible for 17% of the petroleum consumption in the transportation sector. Given the same route, different driving profiles are implemented by truck drivers (speed and gear applied) which result in a large variation in fuel consumption [2]. This implies that optimizing the driving profile has a huge potential for saving fuel. Prior works on this topic typically focused on a single vehicle. Early works [3] described the problem using optimal control framework and derived a necessary condition for optimality using *Pontryagin's maximum principle*, while recent works [4,5,6,7,8] used dynamic programming to solve an approximate optimization problem numerically. In [9] the solution was derived analytically for simplified models. Other works focused on forming vehicle platoons in order to save fuel [10]. In [11] traffic signal information was incorporated in the optimization framework while in [12] traffic volume, density and speed prediction from a macroscopic traffic model was used.

In this paper, we present a modeling framework that allows one to optimize the driving profile to achieve better fuel economy given the elevation profile, headwind, and traffic information along the route. The main progress beyond most recent works [8,11,13] are the following: (1) We incorporate the terminal time in the objective function. Tuning the weight of this term provides a simple way to include traffic information in the optimization; (2) We consider gear changes in fuel optimization; (3) We consider more practical elevation profiles since our framework is applicable for general terrain; (4) Our mathematical approach guarantees that the optimal solution can be found in a fast manner. In particular, to solve the optimal control problem we seek solution of the corresponding boundary value problem (BVP). We first solve a simplified problem analytically and then use numerical continuation to gradually change the parameters until reaching the original nonlinear problem. By doing so, optimality can be guaranteed meanwhile the computation speed increases.

The optimization problem is formulated in Section 2 and we generate the analytical solution of an analogous linear system in Section 3. In Section 4, this solution is used to initialize our numerical continuation software that can produce numerical solu-

*Address all correspondence to this author.

tion of the nonlinear system. In Sections 3 and 4, we investigate how the weight on the terminal time regulates the optimal solutions. Finally, we conclude the paper and propose some future research in Section 5.

## 2 DRIVING PROFILE OPTIMIZATION BASED ON FUEL CONSUMPTION

In this section we lay out a modeling framework that can be used to optimize fuel economy of HDVs. This framework allows the use of different models to describe the vehicle dynamics and a wide variety of fuel consumption maps. In order to keep the problem analytically tractable, we use a simple vehicle model and a static fuel consumption map.

### 2.1 Optimization Problem

The driving profile optimization is formulated as follows. Find the input $a_\mathrm{d}$ to minimize the objective function

$$J_0 = \int_0^{t_\mathrm{f}} q(v, a_\mathrm{d})\,\mathrm{d}t + \sigma_0 \int_0^{t_\mathrm{f}} \mathrm{d}t, \tag{1}$$

subject to the constraints

$$\begin{gathered} \dot{x} = f(x, a_\mathrm{d}), \\ s(0) = 0, \quad s(t_\mathrm{f}) = S, \quad v(0) = v_0, \quad v(t_\mathrm{f}) = v_\mathrm{f}, \\ 0 \le a_\mathrm{d} \le a_\mathrm{U}(v), \end{gathered} \tag{2}$$

where $x = [s, v]^\mathrm{T}$ so that $s$ is the distance (arc-length) traveled, $v$ is the speed of the vehicle, and the dot represents the derivative with respect to time $t$. The initial time is considered to be 0, while the terminal time is denoted by $t_\mathrm{f}$ and it is considered to be unknown. The function $q$ represents the fuel consumption rate and the function $f$ describes the vehicle dynamics. The boundary conditions in the second row of (2) fix the total arc-length of the route $S$, the initial speed $v_0$, and the final speed $v_\mathrm{f}$, while the third row gives a speed-dependent upper bound for the control input $a_\mathrm{d}$. To avoid braking (since it dissipates kinetic energy), we set the control input to be nonnegative.

The first terms of the objective function $J_0$ represents the total fuel consumption

$$Q = \int_0^{t_\mathrm{f}} q\,\mathrm{d}t, \tag{3}$$

while the second term $\sigma_0 t_\mathrm{f}$ represents the total cost corresponding to the terminal time $t_\mathrm{f}$. The parameter $\sigma_0$ is the weight of the latter one, with unit [g/s]. Zero $\sigma_0$ gives a traditional driving profile optimization which is widely studied in the literature. Considering nonzero $\sigma_0$ represents the ability to get to the destination at a given time. Also, it may provide a simple way to incorporate traffic information by using smaller $\sigma_0$ for heavier traffic.

### 2.2 Vehicle Dynamics

The longitudinal dynamics of the HDV is derived using classical mechanics, with assumption that no slip occurs on the wheels and that the flexibility of the tires and the suspension can be neglected. Then using the power law we obtain

$$m_\mathrm{eff}\dot{v} = -mg\sin\phi - \gamma mg\cos\phi - k(v + v_\mathrm{w})^2 + \frac{\eta}{R}T_\mathrm{e}, \tag{4}$$

see [10,14], where the effective mass $m_\mathrm{eff} = m + I/R^2$ contains the mass of the vehicle $m$, the moment of inertia $I$ of the rotating elements, and the wheel radius $R$. Furthermore, $g$ is the gravitational constant, $\phi$ is the inclination angle, $\gamma$ is the rolling resistance coefficient, $k$ is the air drag constant, $v_\mathrm{w}$ is the speed of the headwind, $\eta$ is the gear ratio (that includes the final gear ratio and the transmission efficiency), and $T_\mathrm{e}$ is the engine torque. See Appendix A for parameter values used in this paper. When units are not spelled out, quantities should be understood as SI units.

Eq. (4) can be rewritten as

$$\begin{aligned} \dot{s} &= v, \\ \dot{v} &= -\alpha\sin\phi - \beta\cos\phi - \kappa(v + v_\mathrm{w})^2 + a_\mathrm{d}, \end{aligned} \tag{5}$$

where

$$\alpha = \frac{mg}{m_\mathrm{eff}}, \quad \beta = \frac{\gamma mg}{m_\mathrm{eff}}, \quad \kappa = \frac{k}{m_\mathrm{eff}}, \quad a_\mathrm{d} = \frac{\eta T_\mathrm{e}}{m_\mathrm{eff}R}. \tag{6}$$

Corresponding to (2), the state variables are $s$ and $v$. The control input is the rescaled torque $a_\mathrm{d}$, with unit of acceleration $\mathrm{m/s^2}$. Here we consider $a_\mathrm{d}$ as a independent variable (to be designed) and by choosing the appropriate gear ratio $\eta$ we can calculate how much engine torque $T_\mathrm{e}$ we demand.

In order to obtain the inclination angle $\phi$, we need to define the elevation profile first. Consider that $h(s)$ gives the elevation as a function of distance traveled $s$. In practice, elevation is given as a function of the direct distance $d$. The relationship between $s, d$ and $h$ is illustrated in Figure 1. It can be seen that $h'(s) = \sin\phi$ and $h'(d) = \tan\phi$. One needs the arc-length parameterization $d(s)$ to obtain $h(s)$, but since $\phi < 0.05$ [rad] here we use the approximation $\cos\phi \approx 1$. Moreover, for simplicity we consider no headwind $v_\mathrm{w} = 0$. Thus, (5) can be simplified to

$$\begin{aligned} \dot{s} &= v \\ \dot{v} &= -\alpha h'(s) - \beta - \kappa v^2 + a_\mathrm{d}. \end{aligned} \tag{7}$$

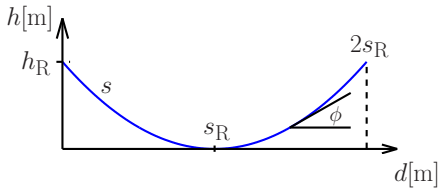


**FIGURE 1**. Elevation $h$ as function of distance $d$ and arc-lengths $s$.

Throughout this paper, we use simple elevation profile

$$h(s) = h_{\mathrm{R}} \left( \frac{s - s_{\mathrm{R}}}{s_{\mathrm{R}}} \right)^2, \tag{8}$$

that is shown in Figure 1. We also consider $h_R \ll s_R$, in particular we use $h_{\mathrm{R}} = 30$ [m], $2s_{\mathrm{R}} = 4000$ [m]. We emphasize that using $a_{\mathrm{d}}$ as the control input enables us to decouple the optimization of the speed profile and the gear selection: the rescaled torque $a_{\mathrm{d}}$ is derived first and then the gear is selected to minimize fuel consumption.

### 2.3 Fuel Consumption Map

The functional (1) contains map $q(v, a_{\mathrm{d}})$ that specifies the fuel consumption rate (with unit [g/s]) for a given input $a_{\mathrm{d}}$ and a given speed $v$. Fuel consumption maps are typically given as a function of the engine speed $\omega_{\mathrm{e}}$ and engine torque $T_{\mathrm{e}}$, that is, $q(\omega_{\mathrm{e}}, T_{\mathrm{e}})$. Dividing this with the engine power $P = T_{\mathrm{e}}\omega_{\mathrm{e}} = m_{\mathrm{eff}} a_{\mathrm{d}} v$ we obtain the brake specific fuel consumption (BSFC):

$$\mathrm{BSFC} = \frac{q(\omega_{\mathrm{e}}, T_{\mathrm{e}})}{T_{\mathrm{e}}\omega_{\mathrm{e}}} = \frac{q(v, a_{\mathrm{d}})}{m_{\mathrm{eff}} a_{\mathrm{d}} v}, \tag{9}$$

where we used $a_{\mathrm{d}} = \frac{\eta T_{\mathrm{e}}}{m_{\mathrm{eff}} R}$ and $v = \frac{R\omega_{\mathrm{e}}}{\eta}$, cf. (6). Small BSFC values imply good fuel economy [15]. Previous efforts on fuel economy optimization usually assumed fixed gear ratio, which resulted in a one-to-one relationship between $q(\omega_{\mathrm{e}}, T_{\mathrm{e}})$ and $q(v, a_{\mathrm{d}})$ [9,11]. In this paper, we generate a map with gear changes involved.

Given a control input $a_{\mathrm{d}}$ at a certain speed $v$, different gears set the engine at different working points, and therefore, yield different BSFC values. We choose the gear that gives the least BSFC among all the available gears and generate the working zone for each gear in the $(v, a_{\mathrm{d}})$ plane as shown in Figure 2(a) for a MaxxForce 13 diesel engine with a 10-speed manual transmission used in a Prostar truck manufactured by Navistar [16]. It can be shown that for any given $(v, a_{\mathrm{d}})$ point, there is a single optimal gear ratio, so one can map the fuel consumption $q$ from the $(\omega_{\mathrm{e}}, T_{\mathrm{e}})$ plane to the $(v, a_{\mathrm{d}})$ plane using the associated gear, which is shown by the contours in Figure 2(b). It can be observed that the contours of fuel consumption map are similar to the iso-power curves ($P = m_{\mathrm{eff}} a_{\mathrm{d}} v$). To obtain an analytical model we fit

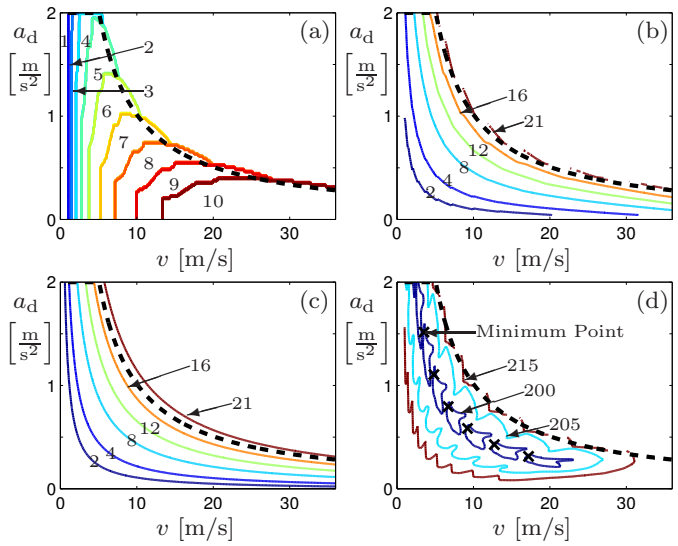


**FIGURE 2**. Contours in the plane of speed $v$ and control input $a_{\mathrm{d}}$. (a) Optimal gear ratios; (b) Experimental fuel consumption contours, with units [g/s]; (c) Fitted fuel consumption contours, with units [g/s]; (d) BSFC with optimal gear ratios applied, with units [kg/(kW · h)]. The black crosses represent points with minimal BSFC value. In all four panels, the black dashed curve is the iso-power line that must not be exceeded in order to keep the engine in the accessible range for all gears.

the data using Willians approximation [17]

$$q(v, a_{\mathrm{d}}) = p_2 v a_{\mathrm{d}} + p_4 v + p_6, \tag{10}$$

by applying least square fitting method [18] and obtained $p_2 = 1.8284 \pm 0.0019\,[\mathrm{gs^2/m^2}]$, $p_4 = 0.0209 \pm 0.0006\,[\mathrm{g/m}]$, $p_6 = -0.1868 \pm 0.0068\,[\mathrm{g/s}]$. The corresponding contours are shown in Figure 2(c).

We assume that gear changes occur instantaneously and the engine's working point jumps along iso-power curves during gear change. The blank regions in Figure 2 correspond to $(v, a_{\mathrm{d}})$ combinations that are not accessible by the engine. This provides a constraint on $a_{\mathrm{d}}$, i.e., give $a_{\mathrm{U}}(v)$ in (2). In particular, if the state of the vehicle is in the region above the black dashed iso-power curve, gear changes may lead to engine states that are not accessible. Therefore, the black dashed curve is the maximum power $P_{\max}$ that the engine may produce in any gear. Note that $P = T_{\mathrm{e}}\omega_{\mathrm{e}} = m_{\mathrm{eff}} a_{\mathrm{d}} v$, and thus, we have

$$a_{\mathrm{U}}(v) = \min\{a_{\max}, U/v\}, \quad \text{where} \quad U = \frac{P_{\max}}{m_{\mathrm{eff}}}. \tag{11}$$

In this paper we use $a_{\max} = 2$ [m/s], $P_{\max} = 300.65\,[\mathrm{kW}] \Rightarrow U = 10.14\,[\mathrm{m^2/s^3}]$ that are acquired through fitting.

### 2.4 Formulating the Boundary Value Problem

Substituting (10) into (1), we obtain

$$J_0 = \int_0^{t_\mathrm{f}} (p_2 v a_\mathrm{d} + p_4 v + p_6 + \sigma_0)\,\mathrm{d}t. \tag{12}$$

Since $p_4 v$ is independent of the control input $a_\mathrm{d}$ and $\int_0^{t_\mathrm{f}} p_4 v\,\mathrm{d}t = p_4 S$ is constant, these terms may be dropped. We define $\sigma = p_6 + \sigma_0$, drop the subscript of $p_2$, and redefine the cost function

$$J = \int_0^{t_\mathrm{f}} p a_\mathrm{d} v\,\mathrm{d}t + \sigma t_\mathrm{f}. \tag{13}$$

Given the optimal control problem (2,7,13), we apply *Pontryagin's maximum principle* [19] to get a necessary condition for the optimal trajectory. First, we define the augmented Hamiltonian

$$\begin{aligned} H(s,v,\lambda,\mu,a_\mathrm{d}) = {} & p v a_\mathrm{d} + \sigma + \lambda v + \mu\big(-\alpha h'(s) - \beta - \kappa v^2 + a_\mathrm{d}\big) \\ & + \nu_1 a_\mathrm{d}/a_\mathrm{U}(v) + \nu_2(1 - a_\mathrm{d}/a_\mathrm{U}(v)), \end{aligned} \tag{14}$$

where $\lambda$ and $\mu$ are the costates, with units [g/m] and [gs/m], respectively. The extra multipliers $\nu_1, \nu_2$ are associated with the constraints in the last row of (2) and they are nonzero only when equalities occur. We will use the vector notation

$$X = [s, v, \lambda, \mu]^\mathrm{T}. \tag{15}$$

We convert the optimal control problem (2,7,13) into a free terminal time boundary value problem (BVP)

$$\begin{bmatrix} \dot{s} \\ \dot{v} \\ \dot{\lambda} \\ \dot{\mu} \end{bmatrix} = \begin{bmatrix} v \\ -\alpha h'(s) - \beta - \kappa v^2 + a_\mathrm{d} \\ \mu\,\alpha h''(s) \\ -\lambda + 2\mu\kappa v - p a_\mathrm{d} - \nu_1 \partial_v\big(\frac{a_\mathrm{d}}{a_\mathrm{U}(v)}\big) - \nu_2 \partial_v\big(1 - \frac{a_\mathrm{d}}{a_\mathrm{U}(v)}\big) \end{bmatrix} \tag{16}$$

$$\underbrace{\begin{bmatrix} s(t_\mathrm{f}) - s(0) - S \\ v(0) - v_0 \\ v(t_\mathrm{f}) - v_\mathrm{f} \\ H(s(t_\mathrm{f}), v(t_\mathrm{f}), \lambda(t_\mathrm{f}), \mu(t_\mathrm{f}), a_\mathrm{d}(t_\mathrm{f})) \end{bmatrix}}_{\mathbf{B}(X(0),X(t_\mathrm{f}))} = \begin{bmatrix} 0 \\ 0 \\ 0 \\ 0 \end{bmatrix}, \tag{17}$$

where the optimal control $a_\mathrm{d}$ is given by

$$a_\mathrm{d} = \arg\min H(s,v,\lambda,\mu,a_\mathrm{d}). \tag{18}$$

Since $H$ is linear in $a_\mathrm{d}$ (cf. (14)) with coefficient

$$z = pv + \mu, \tag{19}$$

(18) yields

$$a_\mathrm{d}(t) = \begin{cases} a_\mathrm{U}(v(t)) & \text{if} \quad z(t) < 0, \\ a_\mathrm{d}^*(t) & \text{if} \quad z(t) = 0, \\ 0 & \text{if} \quad z(t) > 0. \end{cases} \tag{20}$$

This is a "bang-bang" controller, i.e., the control input switches abruptly between different values. The first case is related to the constraint (11) while in the second case the control input is such that the trajectory is kept in the plane $z = 0$. To reveal how can system dynamics remain in the plane $z = 0$, we give the following remarks.

**Remark 1.** *Assume $\kappa \neq 0$ in* (16) *and that no constraints are applied to control input $a_\mathrm{d}$. Then the necessary and sufficient condition to maintain $z = 0$ is having constant speed $v = \sqrt[3]{\sigma/(2p\kappa)}$, which can be calculated by setting $\dot{v} = 0$ and using (14,16,17,19).*

**Remark 2.** *If the gradient $h'(s)$ is mild, that is, given $v(0) = v(t_\mathrm{f}), h(s),\ v > 0, s \in [0, S]$, we have $0 \leq \alpha h'(s) + \beta + \kappa v^2 < \min\{U/v, a_\mathrm{max}\}$, then the control input $a_\mathrm{d}^*(t) = \alpha h'(v_0 t) + \beta + \kappa v_0^2$ keeps the speed constant while satisfying (20).*

Remarks 1 and 2 yield that traveling with a constant speed on a road of mild elevation may be optimal. This result corresponds to the conclusion of [7,20]. However, when the route is steep, we need to switch between maximum and minimum according to (20).

It is known that there is no general existence and uniqueness conditions for boundary value problems, even for smooth dynamic systems [18]. Therefore, whether a solution exists is unknown when setting up parameter values. While system (16,17,20) consist of smooth subsystems, switches make the system non-smooth. Moreover, varying the parameter $\sigma$ changes the boundary condition (17) according to (14) and slight change in this parameter may result in significant change of the optimal control input. Due to these issues, available BVP solvers cannot be applied to solve the system (16,17,20) directly. Before we apply our own solver, we solve an analogous simplified problem analytically. This allows us to characterize the properties of the optimal solution and we can use the analytical solution to initialize our numerical solver.

## 3 ANALYTICAL SOLUTION OF THE LINEAR DAMPED SYSTEM

In this section, we linearize the BVP (16,17,20) and derive the analytical solution. This allows us to characterize how the optimal solution changes with the parameter $\sigma$. Moreover, the analytical solution will be utilized in Section 4 to initialize the

numerical continuation that is used to solve the original nonlinear BVP (16,17,20).

Here, the air drag is approximated by linear damping, i.e., $\kappa v^2$ is replaced by $\kappa v_0 v$, where $v_0 = v(0)$. Moreover, the constraints on $a_\mathrm{d}$ is given by $0 \le a_\mathrm{d} \le a_\mathrm{U}$ where $a_\mathrm{U}$ is constant such that $a_\mathrm{U} \le a_\mathrm{max}$ (cf. (11)). Thus (16) is substituted by the affine equations

$$\begin{bmatrix} \dot{s} \\ \dot{v} \\ \dot{\lambda} \\ \dot{\mu} \end{bmatrix} = \begin{bmatrix} 0 & 1 & 0 & 0 \\ -2\alpha\frac{h_\mathrm{R}}{s_\mathrm{R}^2} & -\kappa v_0 & 0 & 0 \\ 0 & 0 & 0 & 2\alpha\frac{h_\mathrm{R}}{s_\mathrm{R}^2} \\ 0 & 0 & -1 & \kappa v_0 \end{bmatrix} \begin{bmatrix} s \\ v \\ \lambda \\ \mu \end{bmatrix} + \begin{bmatrix} 0 \\ 2\alpha\frac{h_\mathrm{R}}{s_\mathrm{R}} - \beta + a_\mathrm{d} \\ 0 \\ -p a_\mathrm{d} \end{bmatrix}. \tag{21}$$

According to (20), the input $a_\mathrm{d}$ stays at its maximum $a_\mathrm{U}$ or minimum 0 when $z \neq 0$. When $a_\mathrm{d}$ is constant, the dynamics of $s, v$ and the dynamics of $\lambda, \mu$ are decoupled. Therefore, we obtain the solution in the form

$$\begin{bmatrix} s_1 \\ v_1 \\ \lambda_1 \\ \mu_1 \end{bmatrix} = \underbrace{\begin{bmatrix} F_1(s_0, v_0, t_1, a_\mathrm{d}) \\ F_2(s_0, v_0, t_1, a_\mathrm{d}) \\ F_3(\lambda_0, \mu_0, t_1, a_\mathrm{d}) \\ F_4(\lambda_0, \mu_0, t_1, a_\mathrm{d}) \end{bmatrix}}_{\mathbf{F}(X_0, t_1, a_\mathrm{d})}, \tag{22}$$

where we used the abbreviated notation $s(t_1) = s_1$, $v(t_1) = v_1$, $\lambda(t_1) = \lambda_1$, $\mu(t_1) = \mu_1$, $s(0) = s_0$ ,$v(0) = v_0$, $\lambda(0) = \lambda_0$, $\mu(0) = \mu_0$. Note that, when $a_\mathrm{d}$ is not constant but a function of time, we may still get a expression similar to (22), but it becomes a functional. Even though we cannot guarantee that a unique solution exists, we assume that the boundary condition (17) allows at least one solution.

If the system does not satisfy the conditions in Remarks 1 and 2, the control input switches between the cases in (20). In general, there may be multiple switches but in case of the simple elevation profile (8), we only observed one switch. Thus, in this paper we restrict ourselves to this case, i.e., we assume that the trajectory crosses $z = pv + \mu = 0$ once as shown by the trajectories in Figure 3. The control input $a_\mathrm{d}$ either switches from the maximum $a_\mathrm{U}$ to minimum 0 (trajectories 1 and 2), or vice versa (trajectories 3 and 4). Trajectories 1 and 4 are named *traverse scenarios* since these trajectories go through the plane $z = 0$. On the other hand, trajectories 2 and 3 tangentially attach to the plane, travel along it, and leave it after some time. We name these *tangential scenarios*. When the trajectory is tangential to the surface $z = 0$, the control input is $a_\mathrm{d}^*(t) = \alpha h'(s) + \beta + \kappa v_0 v$; see (20) and Remark 2.

By solving the affine equation (21) analytically, the linear system (17,20,21) can be transformed to a system of nonlinear algebraic equations. By using the notation defined in (17,22), for

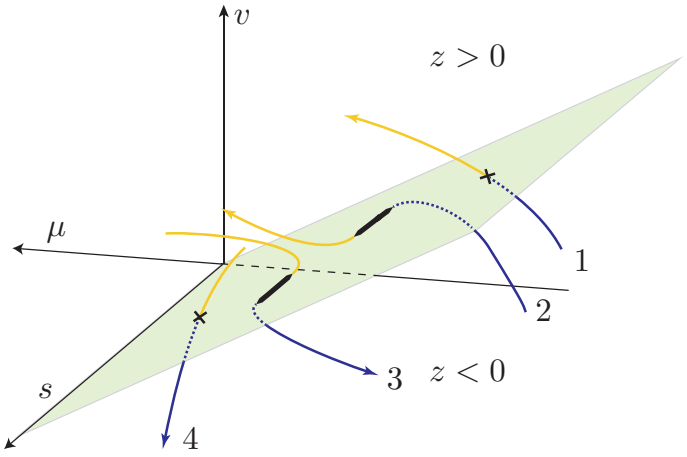


**FIGURE 3**. Four possible scenarios involving one switch. Trajectories 1, 2 are for the case when $a_\mathrm{d}$ switches from maximum to minimum (i.e., $z = pv + \mu$ switches from negative to positive). Trajectory 1 shows a traverse scenario, while trajectory 2 depicts a tangential scenario. Trajectories 3, 4 are for the case when $a_\mathrm{d}$ switches from minimum to maximum (i.e., $z = pv + \mu$ switches from positive to negative). Trajectory 4 represents a traverse scenario, while trajectory 3 shows a tangential scenario. For the tangential scenarios 2 and 3, bold segments correspond to $z = 0$ while for the traverse scenarios 1 and 4, crosses indicate $z = 0$.

the traverse scenario we obtain

$$\begin{aligned} &\mathbf{B}(X_0, X_\mathrm{f}) = \mathbf{0}, \\ &X_1 = \mathbf{F}(X_0, t_1, a_{\mathrm{d}1}), \\ &X_\mathrm{f} = \mathbf{F}(X_1, t_\mathrm{f} - t_1, a_\mathrm{df}), \end{aligned} \tag{23}$$

where $a_{\mathrm{d}1}, a_\mathrm{df} \in \{0, a_\mathrm{U}\}$ such that $a_{\mathrm{d}1} \neq a_\mathrm{df}$. Solving these equations we obtain $t_1, t_\mathrm{f}, \lambda_0, \mu_0$. On the other hand, for the tangential scenario we obtain

$$\begin{aligned} &\mathbf{B}(X_0, X_\mathrm{f}) = \mathbf{0}, \\ &p\dot{v} + \dot{\mu} = 0, \quad \text{for} \quad t \in [t_1, t_2], \\ &X_1 = \mathbf{F}(X_0, t_1, a_{\mathrm{d}1}), \\ &X_\mathrm{f} = \mathbf{F}(X_2, t_\mathrm{f} - t_2, a_\mathrm{df}), \end{aligned} \tag{24}$$

where $a_{\mathrm{d}1}, a_\mathrm{df} \in \{0, a_\mathrm{U}\}$ such that $a_{\mathrm{d}1} \neq a_\mathrm{df}$. Solving these equations we obtain $t_1, t_2, t_\mathrm{f}, \lambda_0, \mu_0$.

Note that, the solutions of (23) and (24) have to be checked whether the initial value $z(0) = pv(0) + \mu(0)$ corresponds to (20). Also, one may obtain solutions such that the speed $v$ becomes negative during the procedure, which is not physically realistic. Moreover, (24) may result solutions which require that $a_\mathrm{d}$ violates the constraint $0 \le a_\mathrm{d} \le a_\mathrm{U}$ in order to maintain $z = 0$. Such solutions may occur for certain parameters $S, v_\mathrm{f}, v_0, a_\mathrm{max}$, but we do not study these cases in this paper.

Now we investigate how the solutions change with the parameter $\sigma$. Our particular interest is how the solution switches between the different types of trajectories shown in Figure 3. We first introduce some critical values for $\sigma$. The change between scenarios 1 and 2 happens when $z(t_1) = 0$, $\dot{z}(t_1) = 0$ hold, which occurs at the critical value $\sigma_{\rm cr1}$. The same condition can be used to find $\sigma_{\rm cr2}$ where the system changes between scenarios 3 and 4. We introduce the critical value $\sigma_{\rm cr3}$, corresponding to the change between scenarios 1 and 4, which occurs when the objective function (13) takes the same value. Denoting the corresponding switching times by $t_1^{(1)}, t_{\rm f}^{(1)}$ and $t_1^{(4)}, t_{\rm f}^{(4)}$, we obtain

$$\int_0^{t_1^{(1)}} a_{\rm U} v \, {\rm d}t + \sigma_{\rm cr3} t_{\rm f}^{(1)} = \int_{t_1^{(4)}}^{t_{\rm f}^{(4)}} a_{\rm U} v \, {\rm d}t + \sigma_{\rm cr3} t_{\rm f}^{(4)}. \qquad (25)$$

Typically, one of the scenarios has less fuel consumption while the other has shorter traveling time. For scenario 1 the input $a_{\rm d}$ switches from $a_{\rm U}$ to 0, while for scenario 4, it switches from 0 to $a_{\rm U}$. Thus scenario 1 has shorter traveling time while 4 has less fuel consumption, since speeding up at the first part will result in a larger average speed. However, for negative values of $\sigma_{\rm cr3}$, shorter traveling time happens to have less fuel consumption as well.

Depending on the relationship between $\sigma_{\rm cr1}, \sigma_{\rm cr2}$ and $\sigma_{\rm cr3}$, we have the following possibilities:

1. For $\sigma_{\rm cr1} < \sigma_{\rm cr2}$, the change between 1 and 4 happens at $\sigma_{\rm cr3}$. Then 1 is the optimal solution for $\sigma > \sigma_{\rm cr3}$ and 4 is the optimal solution for $\sigma < \sigma_{\rm cr3}$.
2. For $\sigma_{\rm cr1} > \sigma_{\rm cr2}$, the dynamics is more complicated. If $\sigma > \max\{\sigma_{\rm cr1}, \sigma_{\rm cr3}\}$ then the optimal solution is 1; if $\sigma < \min\{\sigma_{\rm cr2}, \sigma_{\rm cr3}\}$ then the optimal solution is 4; if $\min\{\sigma_{\rm cr2}, \sigma_{\rm cr3}\} \le \sigma \le \max\{\sigma_{\rm cr1}, \sigma_{\rm cr3}\}$ then the optimal solution is 2 or 3 or some more complicated multiple switch solution, whichever minimizes the objective function (13). We refer to this $\sigma$ domain as the "undetermined range".

As an example, we consider a specific problem where $v(t_{\rm f}) = v(0) = 25\,[{\rm m/s}]$, $a_{\rm U} = 0.6\,[{\rm m/s^2}]$. The critical values are $\sigma_{\rm cr1} = 12.73\,[{\rm g/s}]$, $\sigma_{\rm cr2} = 1.05\,[{\rm g/s}]$, $\sigma_{\rm cr3} = 5.06\,[{\rm g/s}]$, that is, the undetermined range is $[\sigma_{\rm cr2}, \sigma_{\rm cr1}]$. The terminal time $t_{\rm f}$ and total fuel consumption $Q$ are plotted in Figure 4 as a function of $\sigma$. The corresponding time profiles for the points A, B, C are shown in Figure 6. Here the analytical solutions are depicted as red dashed curves while the numerical solutions, obtained by 4th order Runge-Kutta method, are shown as blue solid curves. In all figures, the analytical and numerical solutions are almost undistinguishable from each other. Notice that for case B a section of the trajectory is tangent to the $z = 0$. In cases B and C the peak speed may be too high to be realistic due to the fact that linear air drag is considered and no speed dependent constraint is applied.

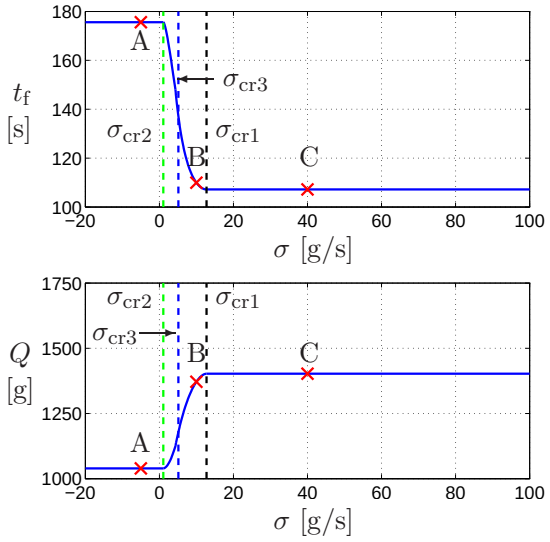


**FIGURE 4**. The upper panel gives the terminal time $t_{\rm f}$ as a function of $\sigma$, while the lower panel shows the fuel consumption $Q$ as a function of $\sigma$, for $v(t_{\rm f}) = v(0) = 25\,[{\rm m/s}]$, $a_{\rm U} = 0.6\,[{\rm m/s^2}]$. The green vertical dashed-dotted line denotes $\sigma_{\rm cr2}$, the black vertical dashed line denotes $\sigma_{\rm cr1}$, and the blue dashed line denotes $\sigma_{\rm cr3}$. The time evolution of the system is shown in Figure 6 for the points marked (A) $\sigma = -5$ [g/s], (B) $\sigma = 10$ [g/s], (C) $\sigma = 40$ [g/s].

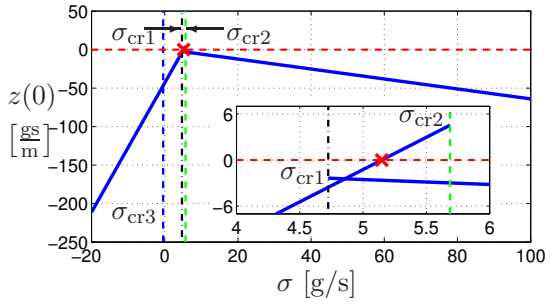


**FIGURE 5**. The initial value of the switching variables $z(0)$ is shown as a function of parameter $\sigma$ for $v(0) = 10[{\rm m/s}]$, $v(t_{\rm f}) = 30[{\rm m/s}]$, $a_{\rm U} = 1[{\rm m/s^2}]$. The critical values $\sigma_{\rm cr1}$, $\sigma_{\rm cr2}$, $\sigma_{\rm cr3}$ are highlighted. The horizontal red dashed line is at $z(0) = 0$ and it intersects with the left branch corresponding to scenario 4 at the red cross.

When nonlinearities are added later in Section 4, the peak speed will reduce to realistic values.

Although there are other possibilities theoretically (e.g. $\sigma_{\rm cr3} > \sigma_{\rm cr1}$), we did not observe such cases under realistic circumstances. However, we remark that the optimal solution may be absent for certain $\sigma$ values. In order to make (20) hold while varying $\sigma$, the sign of $z(0)$ must match with control action (20), i.e., we want $z(0) < 0$ for scenarios 1 and 2 and $z(0) > 0$ for

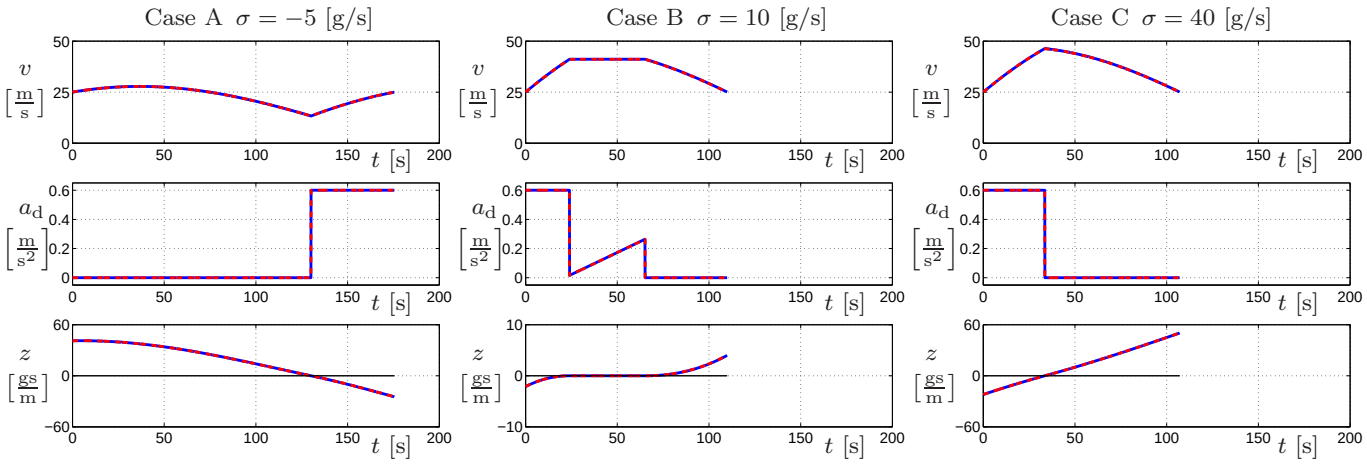


**FIGURE 6**. Time evolution of the speed $v$ (top row), the corresponding control input $a_\mathrm{d}$ (middle row), and the switching variable $z$ (bottom row) for different values of the parameters $\sigma$ as indicated. The columns correspond to the points A, B, C marked in Figure 4. Red dashed curves represent analytical solutions while blue solid curves represent numerical solutions and they match very well.

scenarios 3 and 4 (see Figure 3). For example, if (20) is violated, (23) may not generate a solution with one switch. As an example, we consider $v(0) = 10\,[\mathrm{m/s}], v(t_\mathrm{f}) = 30\,[\mathrm{m/s}], a_\mathrm{max} = 1\,[\mathrm{m/s^2}]$, that yield the critical values $\sigma_\mathrm{cr1} = 4.72\,[\mathrm{g/s}], \sigma_\mathrm{cr2} = 5.69\,[\mathrm{g/s}], \sigma_\mathrm{cr3} = -0.43\,[\mathrm{g/s}]$. Since $\sigma_\mathrm{cr3} < \sigma_\mathrm{cr1} < \sigma_\mathrm{cr2}$, there is no undetermined range, i.e., only scenarios 1 and 4 are possible. The initial value of the switching variable $z(0)$ can be obtained by solving (17,19,23), and it is shown as a function of parameter $\sigma$ in Figure 5. The left branch with positive slope corresponds to scenario 4 (i.e., $a_\mathrm{d}$ switches from 0 to $a_\mathrm{U}$) while the right branch with a negative slope corresponds to scenario 1 (i.e., $a_\mathrm{d}$ switches from $a_\mathrm{U}$ to 0). Indeed, trajectory 4 shall be the optimal solution for $\sigma \le \sigma_\mathrm{cr3}$ while trajectory 1 shall be the optimal solution for $\sigma \ge \sigma_\mathrm{cr3}$. However, on the left of the red cross, we have $z(0) < 0$, that is, scenario 4 violates (20), and thus, it must be discarded. Moreover, scenario 1 only exists for $\sigma > \sigma_\mathrm{cr1}$. Since $\sigma_\mathrm{cr1} > \sigma_\mathrm{cr3}$, we can conclude that for $\sigma < \sigma_\mathrm{cr1}$ then there exist no optimal solution, while for $\sigma > \sigma_\mathrm{cr1}$, scenario 1 is the optimal solution.

## 4 NUMERICAL SOLUTION OF THE NONLINEAR PROBLEM

In this section we solve the original nonlinear BVP (16,17,20) using numerical continuation. This technique was originally developed to compute solutions of systems of parameterized nonlinear equations [21]. We adapt the idea here to track the solutions of BVPs while varying parameters starting from the solution of the simplified equations (17,20,21). Besides the nonlinear "bang-bang" controller (20), the original problem also has two other types of nonlinearity: air drag in (16) and nonlinear input constraint $a_\mathrm{U}(v)$ in (11). The idea is to add these nonlinearities gradually to the linear damped system by varying system parameters.

The nonlinear air drag term is added by varying $\tilde{\kappa}$ from 0 to $\kappa$ in

$$\tilde{\kappa} v^2 + (\kappa - \tilde{\kappa}) v_0 v. \tag{26}$$

To introduce the input constraint (11), we start from $U = v_\mathrm{max} a_\mathrm{max} = 50\mathrm{m/s} \times 2\mathrm{m/s^2}$ and decrease it until we reach $U = P_\mathrm{max}/m_\mathrm{eff} = 10.14[\mathrm{m^2/s^3}]$. Then we change the maximum acceleration gradually from $a_\mathrm{U} = 0.6[\mathrm{m/s^2}]$ to $a_\mathrm{max} = 2[\mathrm{m/s^2}]$. Thus, we end up with solving a series of subproblems, where every solution serves as the initial guess to the next subproblem.

However, continuation cannot be applied for nonsmooth systems. Thus, we derive an approximate system by smoothing system (16,17,20). Specifically, the smoothed version of constraint (11) is written as

$$a_\mathrm{U}(v) = \frac{a_\mathrm{max} + U/v}{2} - \frac{(a_\mathrm{max} - U/v)^2}{2\sqrt{\varepsilon_1 + (a_\mathrm{max} - U/v)^2}}, \tag{27}$$

while the smoothed version of the switching rule (20) can be written as

$$a_\mathrm{d} = \frac{1}{2} a_\mathrm{U}(v) \left(1 - \frac{z}{\sqrt{\varepsilon_2 + z^2}}\right), \tag{28}$$

where $\varepsilon_1$ and $\varepsilon_2$ are small parameters, with units $[\mathrm{m^2/s^4}]$ and $[\mathrm{g^2 s^2/m^2}]$, respectively. The results are visualized in Figure 7, where we compare the nonsmooth formulae (11,20) (red dashed

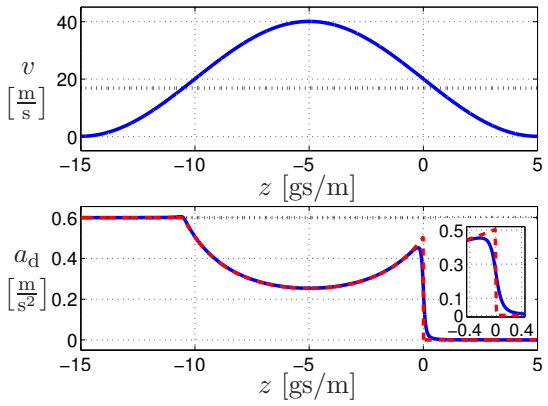


**FIGURE 7**. Visualizing the effect of smoothing. The upper panel shows the speed of the truck as a function of the switching variable $z$. The horizontal dotted line is at $v = U/a_{\max}$. The lower panel depicts the control input. The horizontal black dotted line indicates the maximum control input $a_{\max}$, the red dashed curve is the "bang-bang" controller input (11,20) and the blue solid curve is the smoothed control input (27,28). Here we use $U = P_{\max}/m_{\text{eff}} = 10.14\,[\text{m}^2/\text{s}^3]$, $a_{\max} = 0.6[\text{m}/\text{s}^2]$, $\varepsilon_1 = 0.001[\text{m}^2/\text{s}^4]$, and $\varepsilon_2 = 0.01[\text{g}^2\text{s}^2/\text{m}^2]$.

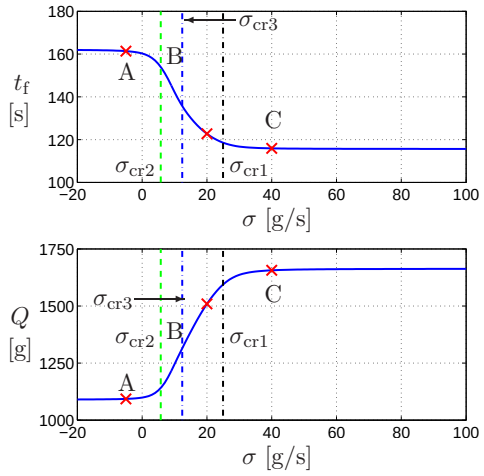


**FIGURE 8**. The terminal time $t_{\text{f}}$ (upper panel) and the fuel consumption $Q$ (lower panel) as a function of $\sigma$ for $v(t_{\text{f}}) = v(0) = 25\,[\text{m}/\text{s}]$. The critical values $\sigma_{\text{cr1}}, \sigma_{\text{cr2}}, \sigma_{\text{cr3}}$ are highlighted. The corresponding trajectories are shown in Figure 9 for the points marked (A) $\sigma = -5\,[\text{g}/\text{s}]$, (B) $\sigma = 10\,[\text{g}/\text{s}]$, (C) $\sigma = 40\,[\text{g}/\text{s}]$.

curve) to the smoothed ones (27,28) (blue solid curve). The horizontal black dotted line in the upper panel is at $v = U/a_{\max}$. When $v$ is below this line, (11) gives $a_{\text{d}} = a_{\max}$, otherwise it gives $a_{\text{d}} = U/v$. The effect of the speed profile can be seen in the lower panel when $z < 0$. Here the horizontal dotted line indicates $a_{\text{d}} = a_{\max}$. This panel also illustrates that for $z < 0$ (20) gives $a_{\text{d}} = a_{\text{U}}(v)$ while for $z > 0$ it gives $a_{\text{d}} = 0$. Notice that for the small $\varepsilon_1, \varepsilon_2$ values used (see caption) the smoothed controller gives a good approximation of the nonsmooth one.

Our BVP solver is based on the shooting method [18], a simple, straightforward, and widely used method that is applicable when the initial values of costates $\lambda(0), \mu(0)$ and the terminal time $t_{\text{f}}$ are unknown. We apply Newton iterations so that we vary the initial conditions and solve the corresponding initial value problem (IVP) by numerical integration. As the Newton iterations converge, the solution approaches the optimal one which satisfies the boundary conditions at the terminal time. Thus, the shooting method transforms the BVP into a system of algebraic equations with unknown variables $\lambda(0), \mu(0), t_{\text{f}}$. In the solver we use the Newton trust region method to solve the nonlinear algebraic equations [22].

Following the results shown in Figures 4 and 6, we solve the nonlinear problem for the same parameter values and plot the terminal time $t_{\text{f}}$ and the total fuel consumption $Q$ as function of $\sigma$ in Figure 8. The critical values are $\sigma_{\text{cr1}} = 24.98\,[\text{g}/\text{s}]$, $\sigma_{\text{cr2}} = 5.75\,[\text{g}/\text{s}]$, and $\sigma_{\text{cr3}} = 12.78\,[\text{g}/\text{s}]$. Recall that if $\sigma < \sigma_{\text{cr2}}$ or $\sigma > \sigma_{\text{cr1}}$, the analytical results suggest that the optimal solution is given by a traverse scenario. This feature remains the same for nonlinear system. However for $\sigma_{\text{cr2}} < \sigma < \sigma_{\text{cr1}}$, the linear approximation predicts a tangential solution while this does not hold for nonlinear system.

The time evolution of the system is shown in Figure 9 for (A) $\sigma = -5\,[\text{g}/\text{s}]$, (B) $\sigma = 10\,[\text{g}/\text{s}]$, (C) $\sigma = 40\,[\text{g}/\text{s}]$. Here blue solid curves represent the trajectories acquired by the our BVP solver based on the smoothed controller (27,28), while the red dashed curves represent the nonsmooth trajectories when applying the "bang-bang" controller (11,20) with the same initial conditions and $t_{\text{f}}$ values. The numerical solution of the nonlinear system maintains the same trend as the analytical solution of the linear system. In cases A and C, the two approaches give very similar results (cf. Figures 6 and 9). But the nonlinear solutions tend to apply maximum control for longer time intervals, due to larger air drag, and smaller maximum torque available. In case B only the trajectories of the system with smooth controller are shown, because the trajectories with nonsmooth controller deviate significantly from the target at the terminal time. Within the undetermined range $[\sigma_{\text{cr2}}, \sigma_{\text{cr1}}]$, the smoothed controller may lead to more complicated switching scenarios for the nonlinear system.

We summarize our results in Table 1, where we show the terminal time $t_{\text{f}}$ and the total fuel consumption $Q$ for different $\sigma$ values for $v(0) = v(t_{\text{f}}) = 25$ [m/s]. For comparison, we also show the results for constant speed (that can be maintained using standard cruise control). When $\sigma$ is small the optimal solution consumes approximately 11.9% less fuel compared to the constant speed scenario. On the other hand, when the weight on terminal time is large and the truck terminates earlier but consumes more fuel. We remark that in order to maintain the constant speed, braking and large engine torque may be needed (i.e., (11) may

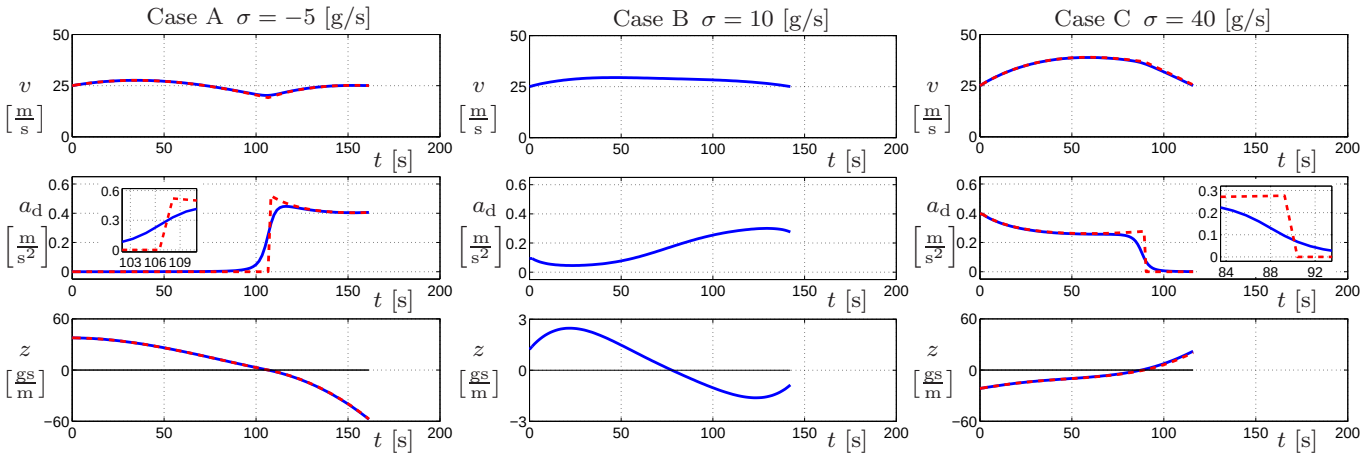


**FIGURE 9**. Time evolution of the speed $v$ (top row), the corresponding control input $a_\mathrm{d}$ (middle row), and the switching variable $z$ for different values of the parameter $\sigma$ as indicated. The columns correspond to the points A, B, C marked in Figure 8. Blue solid curves represent trajectories obtained when applying the smoothed controller (27,28) while the red dashed curves are obtained by applying the "bang-bang" controller (11,20) for the same initial conditions.

| | $t_\mathrm{f}$[s] | $Q$[g] |
|---|---|---|
| $\sigma = -5$ (Case A) | 161.6 | 1076.8 |
| $\sigma = 40$ (Case C) | 115.7 | 1670.0 |
| Cruise Control | 160.0 | 1222.3 |

**TABLE 1**. Terminal time $t_\mathrm{f}$ and fuel consumption $Q$ for $v(0) = v(t_\mathrm{f}) = 25$[m/s].

be violated). Therefore the constant speed driving profile is not necessarily in the function space for the optimal control problem. Finally we remark that including the headwind is a natural extension (cf. (5)). Numerical results show that the increase of headwind will increase the time period when maximum available control input shall be applied.

## 5 CONCLUSION AND FUTURE WORK

In this paper we proposed a framework for fuel economy optimization of heavy duty vehicles that can incorporate road elevation, headwind and traffic information. Starting from the analytical solution of a simplified problem, the problem is solved numerically using numerical continuation. It is shown that by varying the cost related to terminal time, the optimal solution may change significantly. This suggest a strategy for tuning the solutions based on traffic information while obtaining this cost in real-time. Future works also include extensions that can handle longer, more complicated, data-based elevation profiles as well as detailed traffic information. We also plan to implement collocation methods for the BVP solver in order to increase computation speed.


## ACKNOWLEDGEMENT

The authors would like to thank the NAVISTAR company for providing the source data used in this paper.


## REFERENCES


[1] Davis, S. C., Diegel, S. W., and Boundy, R. G., 2013. Transportation energy data book: Edition 32. Tech. rep., United States. Department of Energy.

[2] Saltsman, B., 2014. Impacts of connectivity and automation on vehicle operations. Global Symposium on Connected Vehicle and Infrastructure.

[3] Schwarzkopf, A. B., and Leipnik, R. B., 1977. "Control of highway vehicles for minimum fuel consumption over varying terrain". *Transportation Research,* ***11***(4), pp. 279–286.

[4] Hooker, J. N., 1988. "Optimal driving for single-vehicle fuel economy". *Transportation Research Part A: General,* ***22***(3), pp. 183–201.

[5] Monastyrsky, V. V., and Golownykh, I. M., 1993. "Rapid computation of optimal control for vehicles". *Transportation Research Part B: Methodological,* ***27***(3), pp. 219–227.

[6] Lattemann, F., Neiss, K., Terwen, S., and Connolly, T., 2004. "The predictive cruise control: A system to reduce fuel consumption of heavy duty trucks". *SAE Transactions,* ***113***(2), pp. 139–146.

[7] Chang, D. J., and Morlok, E. K., 2005. "Vehicle speed profiles to minimize work and fuel consumption". *Journal of Transportation Engineering,* ***131***(3), pp. 173–182.

[8] Hellström, E., 2010. "Look-ahead control of heavy vehicles". PhD thesis, Linköping University, Sweden.

[9] Fröberg, A., Hellström, E., and Nielsen, L., 2006. "Explicit fuel optimal speed profiles for heavy trucks on a set of topograhic road profiles". In Proceeding of SAE World Congress.
[10] Alam, A., 2011. "Fuel-efficient distributed control for heavy duty vehicle platooning". PhD thesis, Kungliga Tekniska Högskolan.
[11] Ozatay, E., Ozguner, U., Onori, S., and Rizzoni, G., 2012. "Analytical solution to the minimum fuel consumption optimization problem with the existence of a traffic light". In Proceedings of ASME Dynamic Systems and Control Conference, ASME, pp. 837–846.
[12] Zulkefli, M. A. M., Zheng, J., Sun, Z., and Liu, H., 2013. "Hybrid powertrain optimization with real-time traffic information". In Proceedings of ASME Dynamic Systems and Control Conference, ASME, p. V002T30A005.
[13] Hellström, E., Fröberg, A., and Nielsen, L., 2006. "A real-time fuel-optimal cruise controller for heavy trucks using road topography information". In Proceeding of SAE World Congress.
[14] Orosz, G., and Shah, S. P., 2012. "A nonlinear modeling framework for autonomous cruise control". In Proceedings of ASME Dynamic Systems and Control Conference, ASME, pp. 467–471.
[15] Heywood, J. B., 2002. *Internal combustion engine fundamentals*. McGraw-Hill.
[16] Navistar, 2011. Maxxforce 11 and 13 liter engines. Tech. rep., Navistar Inc.
[17] Guzzella, L., and Onder, C. H., 2004. *Introduction to modelling and control of internal combustion engine systems*. Springer London, Limited.
[18] Stoer, J., Bulirsch, R., Bartels, R., Gautschi, W., and Witzgall, C., 1993. *Introduction to numerical analysis*, Vol. 2. Springer.
[19] Pontryagin, L. S., and Neustadt, L. W., 1962. *The Mathematical Theory of Optimal Processes*, Vol. 4 of *Classics of Soviet Mathematics*. Gordon and Breach Science Publishers.
[20] Hellström, E., 2005. "Explicit use of road topography for model predictive cruise control in heavy trucks". Master's thesis, Linköping University, Sweden.
[21] Allgower, E. E. L., and Georg, K., 2003. *Introduction to numerical continuation methods*, Vol. 45 of *Classics in Applied Mathematics*. SIAM.
[22] Jorge, N., and Wright, S. J., 1999. *Numerical optimization*, Vol. 2. Springer.

## A Parameters used in this paper

| Parameter | Value |
|---|---|
| Mass ($m$) | 29484 [kg] |
| Air Drag Coefficient ($k$) | 3.84 [kg/m] |
| Tire Rolling Radius ($R$) | 0.504 [m] |
| Tire Rolling Resistance Coefficient ($\gamma$) | 0.006 |
| Maximum Acceleration ($a_{\max}$) | 2 [m/s$^2$] |
| Engine Rotational Inertia ($I$) | 39.9 [kg·m$^2$] |
| Gravitational Constant ($g$) | 9.81 [m/s$^2$] |
| Number of Forward Gears | 10 |
| 1st Gear Ratio/Efficiency | 12.94/0.97 |
| 2nd Gear Ratio/Efficiency | 9.29/0.97 |
| 3rd Gear Ratio/Efficiency | 6.75/0.97 |
| 4th Gear Ratio/Efficiency | 4.9/0.97 |
| 5th Gear Ratio/Efficiency | 3.62/0.97 |
| 6th Gear Ratio/Efficiency | 2.64/0.97 |
| 7nd Gear Ratio/Efficiency | 1.90/0.97 |
| 8rd Gear Ratio/Efficiency | 1.38/0.98 |
| 9th Gear Ratio/Efficiency | 1/0.99 |
| 10th Gear Ratio/Efficiency | 0.74/0.98 |
| Final Drive Ratio /Efficiency | 4.17/0.98 |

**TABLE 2**. Data of a 2012 Navistar Prostar truck [16].